Detection of hidden gratings using light and sound

Edward, S.

Publication date
2020
Document Version
Other version
License
Other

2

Theory

2.1 Introduction

The study of materials using femto/picosecond laser-induced high-frequency acoustic waves is usually referred to as laser-induced ultrasonics, or femto or picosecond ultrasonics. When ultrafast laser pulses (typically < 1 ps in duration) are incident on absorptive solids, some part of the optical energy is absorbed and converted to heat. The rapid heating of the lattice leads to thermal stress, which launches a strain wave propagating in all directions. In this thesis, we mainly focus on the longitudinal acoustic waves in metals generated using femtosecond optical pulses, which are acoustic waves propagating normal to the surface with frequencies in the gigahertz (GHz) to terahertz (THz) range.

An advanced numerical model developed by Hao Zhang, which captures the generation, propagation, and detection of high-frequency acoustic waves by ultrafast laser pulses, is used to simulate the experimentally measured diffracted signals [18]. The model consists of three main parts, (i) absorption of light and the subsequent generation of the acoustic wave, (ii) propagation of the acoustic wave, (iii) detection of the acoustic wave. The

absorption of the femtosecond laser pulse and the subsequent heating and cooling of the electron gas inside a metal layer is described by the well-known Two Temperature Model (TTM) [19–24]. The heating of the lattice calculated from the TTM sets up an isotropic thermal stress, which leads to the generation of the high-frequency acoustic wave. The equation of motion for an isotropic, linear elastic wave is used to describe the propagation of the acoustic wave inside the metal and dielectric layers. Finally, by propagating the complex electric field of the light pulse after the optical excitation by the femtosecond laser pulse, through the sample, we can calculate the diffraction efficiency as a function of time delay. The model calculates the first-order diffracted signal by accounting for the spatially periodic changes in the refractive index due to the thermo-optic effect and the strain-optic effect, and the spatially periodic displacement of the surface. In this chapter, we explain the theory underlying the generation, propagation, and detection of acoustic waves in metal layers, which is used in the numerical model.

2.2 Theory of laser-induced acoustic wave generation, propagation and detection

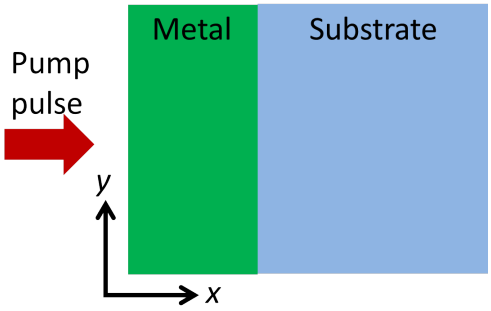

Figure 2.1: Schematic depiction of a metal on a substrate. The laser pulse is incident from x <0. The coordinate directions are used throughout this section.

The model solves a set of time-dependent equations in two spatial dimensions, x and y. In the convention we use, the pump pulse is incident along the x-axis, and when the sample has a buried grating, the k-vector of the grating is along the y-axis (see Figure 2.1).

2.2.1 Acoustic wave generation

The first step in laser-induced ultrasonics is the absorption of the femtosecond pulse, which causes the rapid heating of the lattice. To calculate the intensity of light absorbed inside a thick metal layer, we can use a simple Lambert-Beer law with a correction term for the reflection. This is sufficient to describe laser intensity attenuation inside the sample. Therefore, the intensity of the light inside the layer $I(x, y, t)$ can be written as,

$$I(x, y, t) = (1 - R)I_0(x, y, t)e^{(-x/L)}, \tag{2.1}$$

where R is the reflectivity of the sample, I_0 is the intensity of the incident laser pulse, and L is the optical penetration depth. The optical penetration depth is related to the absorption coefficient α at the pump wavelength by $L = 1/\alpha$. The relation in Eq. 2.1 describes the absorption of the pump light when the thickness of the metal layer is much larger than the optical penetration depth. When the layer thickness is smaller than the optical penetration depth, or for multilayered structures where reflections at each interface must be considered, the transfer matrix method [25, 26] is a more suitable method to calculate the intensity of the absorbed light. If the absorption layer contains sub-wavelength structures, optical near field effects become important, and in this case, a more general method for the solution of Maxwell's equations must be used. After calculating the intensity distribution of light inside the metal, we can calculate the increase in lattice temperature $\Delta T_l(x, y, t)$ using the two-temperature model [19]. The two temperature model, originally proposed by Anisimov et al. [19], is a widely used phenomenological model that describes electron-lattice dynamics after optical excitation with a laser pulse. In this model, the electron gas is assumed to be thermalized at all times during and after excitation and is described by a time-dependent temperature T_e. The lattice is also described as having a time-dependent temperature T_l. For time scales greater than the electron thermalization time (which is smaller than a few hundred femtoseconds for most metals), the two-temperature model provides a good description of the spatial and temporal evolution of electron temperature T_e and lattice temperature T_l. The electron gas and the lattice, exchange energy through electron-phonon coupling, which tends to equilibrate the two temperatures. The equation describing the electron gas temperature

includes a source term $S(x, y, t) = \alpha I(x, y, t)$, which describes when and where energy is deposited in the metal layer by the laser pulse. Initially, the optical energy is absorbed by the electron gas system, increasing the electron temperature while the lattice remains at room temperature. The hot electron gas diffuses into the metal layer and transfers energy to the lattice subsystem, as described by the following coupled equations [27, 28]

$$\begin{aligned} C_e(T_e)\frac{\partial T_e}{\partial t} &= \nabla \cdot K_e \nabla T_e - g(T_e - T_l) + \alpha I(x, y, t), \\ C_l \frac{\partial T_l}{\partial t} &= \nabla \cdot K_l \nabla T_l + g(T_e - T_l), \end{aligned} \tag{2.2}$$

where C_e and C_l are the respective heat capacities of the electron gas and lattice respectively, K_e and K_l denotes the thermal conductivities of the electron gas and the lattice respectively, and g is the electron-phonon coupling constant [27, 28]. The temperature dependence of lattice heat capacity, lattice thermal conductivity as well as electron-phonon coupling strength are neglected as the lattice temperature increase in our experimental conditions is calculated to be only a few tens of K. We use the relations $C_e = A_e T_e$ and $K_e = K_0 \times T_e/T_l$ [21] and solve the TTM numerically to calculate the time evolution of the electron temperature T_e and the lattice temperature T_l. Here, A_e is the electron specific heat constant and K_0 is the thermal conductivity at 273 K.

In metals, the rapid increase of the lattice temperature $T_l(x, y, t)$ sets up an isotropic thermal stress σ^{th} which is the dominant mechanism for acoustic wave generation [29, 30]. This is this source term for the acoustic wave generated in the metal layer. The relation between the thermal stress and lattice temperature change $\Delta T_l(x, y, t)$ is given by,

$$\sigma_x^{th} = \sigma_y^{th} = -3B\beta\Delta T_l(x, y, t), \tag{2.3}$$

where $\sigma_x^{th} = \sigma_y^{th}$ are the two cartesian components of the thermal stress, B is the bulk modulus of the metal and β denotes the linear expansion coefficient. We solve the two-temperature model using Eq. 2.2, to obtain the lattice temperature increase $\Delta T_l(x, y, t)$. With this, we can calculate the thermal stress σ^{th} using Eq. 2.3.

2.2.2 Acoustic wave propagation

The propagation of an acoustic wave in a metal can be described by the equation of motion for an isotropic, linear elastic wave [31, 32] where the source term is given by Eq. 2.3. Therefore, the displacement vector $\vec{u}$ of the material can be written as,

$$\rho\frac{\partial^2\vec{u}}{\partial t^2} = \mu\nabla^2\vec{u} + (\mu+\lambda)\nabla(\nabla\cdot\vec{u}) + \nabla\sigma^{th} \tag{2.4}$$

where ρ is the mass density of the material, λ and μ are the so-called two Lamé parameters in the stress-strain relationship.

Expanding Eq. 2.4 in two-dimensional cartesian coordinate leads to the equations for the velocity components v_x and v_y [18],

$$\begin{aligned}\frac{\partial v_x}{\partial t} &= -\frac{1}{\rho}(\frac{\partial\sigma_x^{re}}{\partial x} + \frac{\partial\sigma_{xy}^{re}}{\partial y} - \frac{\partial\sigma_x^{th}}{\partial x}),\\ \frac{\partial v_y}{\partial t} &= -\frac{1}{\rho}(\frac{\partial\sigma_y^{re}}{\partial y} + \frac{\partial\sigma_{xy}^{re}}{\partial x} - \frac{\partial\sigma_y^{th}}{\partial y}).\end{aligned} \tag{2.5}$$

where, σ_x^{re},σ_y^{re} are the normal stress components and σ_{xy}^{re} is the shear stress. Here,

$$\begin{aligned}\sigma_x^{re} &= -(\lambda+2\mu)s_x - \lambda s_y;\quad \sigma_y^{re} = -(\lambda+2\mu)s_y - \lambda s_x,\\ \sigma_{xy}^{re} &= -\mu s_{xy}.\end{aligned} \tag{2.6}$$

where s_x and s_y are the components of normal strain and s_{xy} the shear strain. The superscript "re" stands for "restoring" as they originate from the restoring force. Eq. 2.6 is known as the strain-stress relation. The definition of normal and shear strain come with the expansion as well, i.e.,

$$s_x = \frac{\partial u_x}{\partial x};\quad s_y = \frac{\partial u_y}{\partial y};\quad s_{xy} = \frac{\partial u_x}{\partial y} + \frac{\partial u_y}{\partial x}. \tag{2.7}$$

The equation of motion described in Eq. 2.4 does not include damping. Acoustic damping is included in the model by adding two viscous terms to the equation of motion [33, 34]. Also, the model we use in the numerical simulations includes relaxation damping [35–37]: the sound waves disturb

the distribution function of the thermal phonons, and the return of the system to equilibrium through phonon collisions removes energy from the sound wave. The details of the model explaining how the various damping terms are added are discussed in [18].

2.2.3 Optical detection of the acoustic wave

In a laser-induced ultrasonics pump-probe experiments, the probe pulse detects the response of the material to the presence of an acoustic wave. This is usually done by measuring changes in the sample reflectivity [38], by measuring diffraction efficiency in the case of transient-grating experiments [39, 40] or by using interferometric measurements [41, 42] where the electric-field amplitude and phase of the probe pulse are measured simultaneously. In our experiments, we measure the change in the intensity of the diffracted probe pulse induced by the pump pulse. Diffraction of the probe pulse can arise due to (i) a spatially periodic displacement of the surface, (ii) a spatially periodic change in the refractive index in a layer near the surface, or (iii) a combination of both effects. A change in the refractive index of a medium due to the presence of an acoustic strain wave is commonly referred to as the strain-optic effect. In addition to this, spatially periodic lattice temperature variations at the surface can also give rise to grating-like changes in the refractive index near the surface. A change in the refractive index of a medium due to a temperature change is commonly referred to as the thermo-optic effect.

The transient change of the refractive index may influence both amplitude and phase of the electric field of the reflected/diffracted probe pulse while the displacement of the surface only changes the phase of the electric field of the reflected/diffracted probe pulse. The change of the refractive index due to the lattice temperature increase, $\Delta\widetilde{n}_T(x, y, t)$, can be expressed in a linear relationship as,

$$\Delta\widetilde{n}_T(x, y, t) = \left(\frac{\partial n}{\partial T} + i\frac{\partial \kappa}{\partial T}\right)\Delta T_l(x, y, t), \tag{2.8}$$

where $\partial n/\partial T$ and $\partial \kappa/\partial T$ are the real and imaginary parts of the thermo-optic coefficient, respectively, and ΔT_l is the lattice temperature increase.

Similarly, the change of the refractive index due to the strain-optic effect, $\Delta\widetilde{n}_s(x,y,t)$, can be expressed as,

$$\Delta\widetilde{n}_s(x,y,t) \quad = \quad \left(\frac{\partial n}{\partial s_x} + i\frac{\partial \kappa}{\partial s_x}\right) s_x(x,y,t). \tag{2.9}$$

where $\partial n/\partial s_x$ and $\partial \kappa/\partial s_x$ are the real and imaginary parts of the strain-optic coefficient respectively and s_x is the longitudinal strain. The two relations in Eq. 2.8 and Eq. 2.9, are valid when the probe pulse is incident normal to the surface and when the strain field doesn't have a large off-axis component ($s_y \approx 0$). If the probe pulse is not incident in a direction normal to the surface, or if the strain field has large off-axis components, the anisotropy of the sound-induced changes in the permittivity tensor should be taken into account. In that case, one has to solve Maxwell's equations in an anisotropic medium to obtain the diffracted/reflected field of the probe pulse. In our experiments, the probe pulse is incident on the surface at almost normal incidence, and the strain-optic effect due to acoustic diffraction is neglected. When the strain-optic and thermo-optic coefficients are known, the total change of the refractive index $\Delta\widetilde{n}(x,y,t) = \Delta\widetilde{n}_T(x,y,t) + \Delta\widetilde{n}_s(x,y,t)$ can be determined. Later, the complex electric field of the probe pulse at the surface, $\widetilde{E}_{p\Delta\widetilde{n}}$, is calculated for each time step using the transfer-matrix method [43].

According to the Fraunhofer diffraction theory, the two dimensional spatial Fourier transform of this electric field should give the far field diffraction pattern. However, we need to include the spatial modulation of this electric field due to the grating-shaped surface displacement from the spatially periodic acoustic wave. It is assumed that the surface displacement by the acoustic wave only introduces a local phase-shift to the electric field. Therefore the complex electric field that takes all the effects into account, $\widetilde{E}_p$, can be written as,

$$\widetilde{E}_p(y,t) = \widetilde{E}_{p\Delta\widetilde{n}}(y,t)e^{i\frac{4\pi n}{\lambda_p}u_{xs}(y,t)}, \tag{2.10}$$

where u_{xs} is the surface displacement as a function of y and $\widetilde{E}_{p\Delta\widetilde{n}}(y,t)$ is the earlier calculated complex electric field of the probe at the surface after accounting for the refractive index changes. The assumption that surface displacement only introduces a phase shift in the electric field is commonly

known as the shallow grating approximation. This is a valid approximation when the peak-to-valley amplitude of the displacement grating is much smaller than the wavelength of the probe pulse (800 nm). This is usually the case for laser-induced ultrasonics experiments where the surface and interface displacement amplitudes are less than a nanometer.

Once we know the complex electric field at the surface that includes any possibles refractive index modulations and possible displacement of the surface, we can take the 2D spatial Fourier transformation to obtain the diffracted electric fields in the far field. The optical intensity of the 1^{st} order diffracted field is then calculated.

In the next section we demonstrate mathematically that when a diffraction grating is translated along the grating vector direction, the $+1^{st}$ order and the -1^{st} order beams acquire opposite phase shifts.

2.3 Fraunhofer diffraction from a displaced grating

We use the Fraunhofer diffraction equation to describe the diffraction of optical fields when the diffraction pattern is viewed at a large distance from the diffracting object. This is the case when we have optical diffraction from a grating. The following is adapted from [44]. The electric field of U, at the far field from a aperture can be described as:

$$U(x,y,z) = \frac{e^{ikz}e^{i\frac{k}{2z}(x^2+y^2)}}{i\lambda z}\iint_{-\infty}^{\infty} U(\xi,\eta,z=0)e^{-i\frac{2\pi}{\lambda z}(x\xi+y\eta)}d\xi d\eta. \quad (2.11)$$

where ξ and η are the source coordinates and x, y, and z, are the coordinates where the field is calculated. Defining the spatial frequencies spatial frequencies as $f_x = x/(\lambda z)$ and $f_y = y/(\lambda z)$, we write Eq. 2.11 as,

$$U(x,y,z) = \frac{e^{ikz}e^{i\frac{k}{2z}(x^2+y^2)}}{i\lambda z}\iint_{-\infty}^{\infty} U(\xi,\eta,z=0)e^{-i2\pi(f_x\xi+f_y\eta)}d\xi d\eta. \quad (2.12)$$

The Eq. 2.12 shows that the diffraction field is related to the source field by a simple Fourier transform relationship. We now define a transmission function t_A which is the ratio of the complex field immediately behind a plane

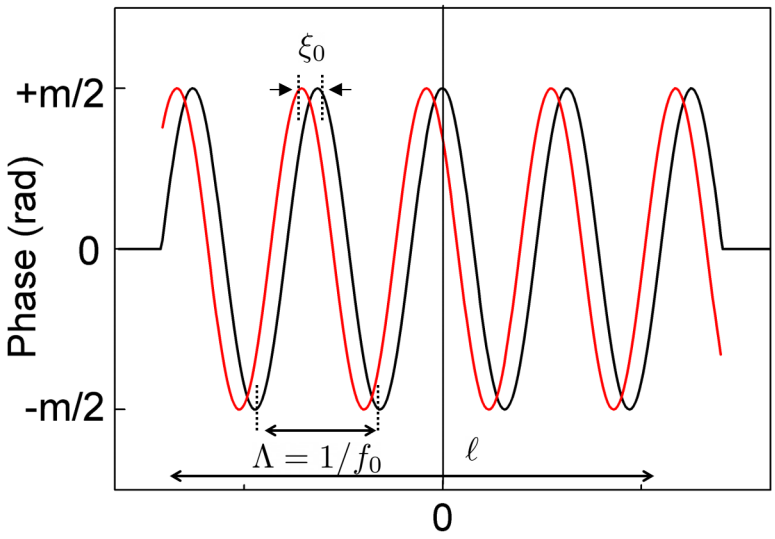

Figure 2.2: An example of a cosine phase grating with grating period Λ (spatial frequency $f_0 = 1/\Lambda$), amplitude $m/2$, and multiplied by a rect function, rect(ξ/ℓ) . The red curve is a grating with the same rect function, but with the phase grating shifted by $-\xi_0$.

to that of the field incident on the plane. If the incident field has amplitude 1 and is incident normally on the screen (so no phase variation across the aperture for the incident beam) then we can write: $t_A(\xi, \eta) = U(\xi, \eta, z = 0)$.

For this calculation we will assume that the grating is a thin cosine phase grating with dimensions in the x and y-direction of ℓ (Figure 2.2). Hence we can write the complex transmission function for this grating as,

$$t_A(\xi, \eta) = \exp\left[i\frac{m}{2}\cos(2\pi f_0(\xi + \xi_0))\right]\text{rect}\left(\frac{\xi}{\ell}\right)\text{rect}\left(\frac{\eta}{\ell}\right), \qquad (2.13)$$

where f_0 is the spatial frequency of the grating, $-\xi_0$ is the distance over which the grating has been displaced compared to the original position (ξ_0 =0) and m is the peak-to-valley variation of the phase.

The Fourier transform will give us the following expression,

$$\begin{aligned}\mathrm{FT}\left[t_A\left(\xi,\eta\right)\right] &= \sum_{q=-\infty}^{\infty}\iint_{-\infty}^{\infty}\ell^2\mathrm{sinc}\left[\ell(f_x-f_1)\right]\mathrm{sinc}\left[\ell(f_y-f_2)\right] \\ &\quad \exp\left(i2\pi f_1\xi_0\right)i^q J_q\left(\frac{m}{2}\right)\delta(f_1-qf_0,f_2)df_1df_2 \\ &= \sum_{q=-\infty}^{\infty} i^q J_q\left(\frac{m}{2}\right)\ell^2\mathrm{sinc}\left[\ell(f_x-qf_0)\right]\mathrm{sinc}\left[\ell f_y\right]\exp\left(i2\pi q f_0\xi_0\right).\end{aligned} \tag{2.14}$$

where, J_q is the Bessel function of the first kind and order q.

Since we are interested it the $+1^{\text{st}}$ and the -1^{st} order diffracted light, we use the value $q=1$ and $q=-1$ to get,

$$U_{q=1}(x,y,z) = \frac{e^{ikz}e^{i\frac{k}{2z}(x^2+y^2)}}{i\lambda z}J_1(\frac{m}{2})\ell^2\mathrm{sinc}[\ell(f_x-f_0)]\mathrm{sinc}[\ell f_y] \exp(2\pi f_0\xi_0+i\frac{\pi}{2}) \tag{2.15}$$

$$U_{q=-1}(x,y,z) = -\frac{e^{ikz}e^{i\frac{k}{2z}(x^2+y^2)}}{i\lambda z}J_{-1}(\frac{m}{2})\ell^2\mathrm{sinc}[\ell(f_x+f_0)]\mathrm{sinc}[\ell f_y] \exp(-i2\pi f_0\xi_0+i\frac{\pi}{2}). \tag{2.16}$$

As expected, the phase terms, $\exp\left(\pm i2\pi f_0\xi_0\right)$ are opposite in phase. Since $J_{-1}\left(\frac{m}{2}\right) = -J_1\left(\frac{m}{2}\right)$, we can write the above expression as,

$$U_{q=1}(x,y,z) = \frac{e^{ikz}e^{i\frac{k}{2z}(x^2+y^2)}}{i\lambda z}J_1(\frac{m}{2})\ell^2\mathrm{sinc}[\ell(f_x-f_0)]\mathrm{sinc}[\ell f_y] \exp(i2\pi f_0\xi_0+i\frac{\pi}{2}) \tag{2.17}$$

$$U_{q=-1}(x,y,z) = \frac{e^{ikz}e^{i\frac{k}{2z}(x^2+y^2)}}{i\lambda z} J_1(\frac{m}{2})\ell^2 \mathrm{sinc}[\ell(f_x+f_0)]\mathrm{sinc}[\ell f_y] \exp(-i2\pi f_0\xi_0 + i\frac{\pi}{2}). \tag{2.18}$$

From the above expression we can see that a translation of the grating along the direction parallel to the grating k vector (ξ_0) changes the phase of the -1^{st} and $+1^{\mathrm{st}}$ order diffracted fields in opposite direction. We can also see that the intensities of the -1^{st} and $+1^{\mathrm{st}}$ order diffracted fields remain the same after the translation.

For a non-displaced cosine grating ξ_0 =0, and the expressions for first-order diffracted electric fields are,

$$U_{q=1}(x,y,z)|_{\xi_0=0} = \frac{e^{ikz}e^{i\frac{k}{2z}(x^2+y^2)}}{i\lambda z} J_1(\frac{m}{2})\ell^2 \mathrm{sinc}[\ell(f_x-f_0)]\mathrm{sinc}[\ell f_y] \exp(i\frac{\pi}{2}) \tag{2.19}$$

$$U_{q=-1}(x,y,z)|_{\xi_0=0} = \frac{e^{ikz}e^{i\frac{k}{2z}(x^2+y^2)}}{i\lambda z} J_1(\frac{m}{2})\ell^2 \mathrm{sinc}[\ell(f_x+f_0)]\mathrm{sinc}[\ell f_y] \exp(i\frac{\pi}{2}) \tag{2.20}$$

Here the phases of the -1^{st} and $+1^{\mathrm{st}}$ order diffracted fields are the same, as expected.

2.4 Transient-grating pump-probe setup

Experiments described in this thesis aim to study the electron-lattice dynamics in metals and to generate grating-shaped acoustic waves in metals, were mostly performed using a transient-grating pump-probe setup. In a

transient-grating pump-probe setup, two pump pulses are crossed at an angle to create an optical interference pattern on the sample. The interference pattern, which has the shape of a grating with a spatial period Λ, excites the sample in a spatially periodic manner. The spatial modulation induced by the interference pattern can result in the diffraction of a delayed probe pulse.

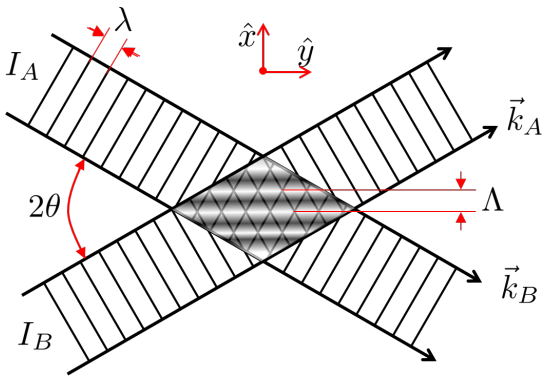

Figure 2.3: Transient-grating produced by two interfering beams with intensities I_A and I_B having wave vectors k_A and k_B respectively.

Here we show the derivation of the transient-grating period Λ, for two plane waves with a wavelength λ crossing at each other at an angle 2θ. A detailed theoretical description of two beam interference under various conditions can be found in here [45]. An experimental configuration for the generation of transient-gratings is shown in Figure 2.3. The output from the laser is split into two beams, denoted here as A and B. The electric field of beams A and B can be written as,

$$\vec{E}_A(\vec{r},t) = E_A \exp[i(\vec{k}_A \cdot \vec{r} - \omega t + \phi_A)]\hat{r} \tag{2.21}$$

and,

$$\vec{E}_B(\vec{r},t) = E_B \exp[i(\vec{k}_B \cdot \vec{r} - \omega t + \phi_B)]\hat{r}, \tag{2.22}$$

respectively, where $\hat{r} = \hat{x} + \hat{y}$. Here, $\vec{k_A}$ and $\vec{k_B}$ are wave-vectors, E_A and E_B are the electric field amplitudes, and ϕ_A and ϕ_B are the optical phases, of beam A and B, respectively. In the coordinate system we use, the wave

vectors can be written as,

$$\begin{aligned} \vec{k}_A &= k\cos\theta\hat{x} + k\sin\theta\hat{y} \\ \vec{k}_B &= k\cos\theta\hat{x} - k\sin\theta\hat{y}. \end{aligned} \tag{2.23}$$

where $k = 2\pi/\lambda$. The two fields interfere on the sample surface and the total electric field due to the interference can be written as,

$$\vec{E}(r,t) = E_A \exp\left[i(\vec{k}_A \cdot \vec{r} - \omega t + \phi_A)\right]\hat{r} + E_B \exp[i(\vec{k}_B \cdot \vec{r} - \omega t + \phi_B)]\hat{r} \tag{2.24}$$

The intensity $I(\vec{r},t)$ of the plane wave is given by the time average of the Poynting vector,

$$I(\vec{r},t) = <\vec{S}> = \frac{\epsilon c n}{2}|\vec{E}(\vec{r},t)|^2 \tag{2.25}$$

where c is the speed of light in vacuum, ϵ is the vacuum permittivity and n is the refractive index of the medium. Since,

$$|\vec{E}(\vec{r},t)|^2 = E_A^2 + E_B^2 + 2E_A E_B \cos(\vec{K}.\vec{r} + \phi_1 - \phi_2) \tag{2.26}$$

where the grating vector $\vec{K}$ is given by,

$$\vec{K} = \pm(\vec{k}_A - \vec{k}_B) = \pm 2k\sin\theta\hat{y}, \tag{2.27}$$

we can write the intensity along the x-axis due to the interfering plane waves as,

$$I = \frac{\epsilon c n}{2}(E_A^2 + E_B^2 + 2E_A E_B \cos(2k\sin\theta + \phi_1 - \phi_2)). \tag{2.28}$$

When the phase difference between the two beams is set to zero: $\phi_A = \phi_B$, the intensity of the interference pattern can be written as,

$$I = I_A + I_B + \frac{\epsilon c n}{2} 2E_A E_B \cos(2k\sin\theta), \tag{2.29}$$

where I_A and I_B are the intensities of the beams A and B respectively. The spatial modulation of the intensity is due to the cosine term in Eq. 2.29 and therefore, the spatial period of the transient grating is then given by,

$$\Lambda = \frac{\lambda}{2\sin\theta} \tag{2.30}$$

where, λ is the pump wavelength and 2θ is the angle between the beams. Here it can be seen that the pitch of the grating can be varied by changing the angle between the beams. The smallest grating pitch that can be achieved is $\lambda/2$ when the angle between the beams is π, and the largest grating pitch that can be achieved is limited by the diameter of the laser beams. In our transient-grating setup, the angle between the beams is such that $\sin\theta = 1/30$, and $\lambda = 400$ nm; therefore, we have a grating period of 6 µm.